Feasibility study for positron emission mammography

C. J. Thompson
Medical Physics Unit and Montreal Neurological Institute, McGill University, 3801 University Street, Montreal, Quebec, Canada

K. Murthy
Medical Physics Unit, McGill University, Montreal, Quebec, Canada

I. N. Weinberg
Department of Radiology, John Hopkins University, Baltimore, Maryland and FM Technologies Inc., Fairfax, Virginia

F. Mako
FM Technologies Inc., Fairfax, Virginia

(Received 6 August 1993; accepted for publication 5 January 1994)

A feasibility study is presented for a small, low-cost, dedicated device for positron emission mammography. Two detector arrays above and below the breast would be placed in a conventional mammography unit. These detectors are sensitive to positron annihilation radiation, and are connected to a coincidence circuit and a multiplane image memory. Images of the distribution of positron-emitting isotope are obtained in real time by incrementing the memory location at the intersection of each line of response. Monte Carlo simulations of a breast phantom are compared with actual scans of this phantom in a conventional PET scanner. The simulations and experimental data are used to predict the performance of the proposed system. Spatial resolution experiments using very narrow bismuth germanate BGO crystals suggest that spatial resolutions of about 2 mm should be possible. The efficiency of the proposed device is about ten times that of a conventional brain scanner. The scatter fraction is greater, but the scattered radiation has a very flat distribution. By designing the device to fit in an existing mammography unit, conventional mammograms can be taken after the injection of the radio-pharmaceutical allowing exact registration of the emission and conventional mammographic images.

Key words: PET, mammography, spatial resolution

I. INTRODUCTION

Conventional mammography provides very-high-resolution images of breast tissue.[1,2] It only detects changes in electron density[3] and is not able to distinguish the biochemical characteristics and metabolic rate of the tissue. Metabolic imaging promises to provide a more specific diagnosis for lesions in which calcifications and scar tissue are visible by mammography. Nuclear medicine can distinguish between tissues which have different metabolic rates after the injection of a suitable tracer. However, detectors used for nuclear medicine cannot easily be positioned to provide registration between the high-resolution electron density image obtained from mammography and the images from a gamma camera. In addition, the resolution of nuclear medicine imaging devices does not scale very well for examination of small organs, as the collimators limit the resolution to about 5 mm. Also, the image contrast is limited by scattered radiation and poor counting efficiency.

Recently there have been several reports of breast tumor detection using positron emission tomography (PET).[3–6] The use of whole body PET scanning for detection of metastases has also been reported.[3] However, PET facilities are still quite rare and the equipment and personnel required for PET are too expensive for routine use. The recently introduced negative ion cyclotrons[7,8] can produce substantial quantities of 18-fluorine. Automatic synthesis units for the production of fluorodeoxyglucose (FDG) should soon make this excellent metabolic tracer more widely available. Enough FDG can now be produced in one batch for ten patient doses. The relatively long half-life (2 h) of FDG makes it suitable for distribution to several sites within a metropolitan area. There should therefore be a readily available source of tracer if a small, easy to use imaging system were available for breast imaging. In addition, several tumor-seeking radio-pharmaceuticals[9–12] have been reported, and these would increase the diagnostic specificity.

The design goals for such an instrument include short imaging time and high resolution. Improved diagnostic specificity is needed in order to reduce the need for surgical biopsies and to allow more confident definition of tumor prior to lumpectomy or biopsy.[13] The use of instruments to assess the metabolism and receptor density noninvasively would be useful in following patients receiving adjunct chemotherapy.[14] The cost of a study on such a unit would have to be less than an equally specific noninvasive diagnostic test in order to justify its use. The cost of the pharmaceutical is expected to come down with increased availability; however, the imaging device must be inexpensive and easy to use to reduce personnel costs.

This feasibility study was undertaken to compare the performance (resolution and sensitivity) of a potential device with a conventional PET scanner. The spatial resolution of any PET scanner gets worse as the detector separation increases since the two gamma rays produced during positron annihilation are not exactly 180° apart. All previous reports of detecting breast lesions with PET used "body scanners" with circular arrays of crystals about 1 m in diameter. There are also brain and animal scanners which are smaller and

 0094-2405/94/21(4)/529/10/$1.20

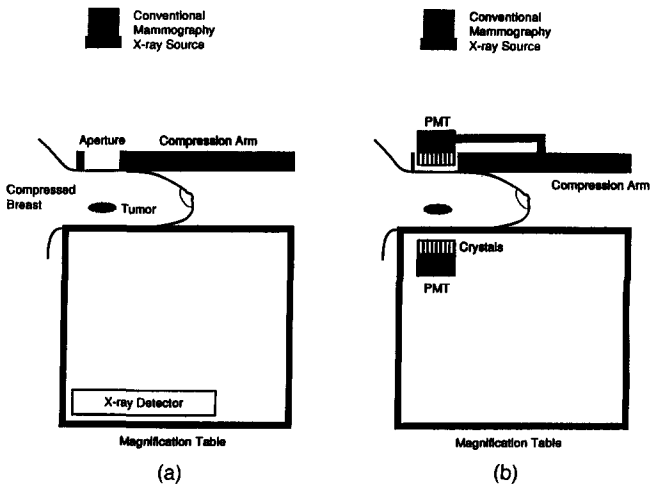

FIG. 1. Schematic of the proposed positron emission mammography device. The device is envisioned as an accessory to fit a conventional mammography gantry (a). After compression, modules containing the detector arrays will be swung into place (b). The distance between the arrays is adjustable.

cheaper, but these are unsuitable for breast imaging. Moving the crystals closer as we propose will reduce this aspect of image blurring. It will also increase the efficiency by making the detectors subtend a greater solid angle, providing better resolution at lower cost. It would normally increase the fraction of scattered radiation detected, but this is offset by the fact that the breast can be compressed substantially, thus reducing the possibility of scattering before detection. There will be a smaller number of rays scattered than with conventional brain or body scanning, but a greater fraction of the rays which are scattered rays will be detected.

Figure 1 shows the general concept of the proposed instrument, with two planar arrays of crystals above and below the compressed breast. The breast compression system from a conventional mammography system is used, but the x-ray source and imaging film are replaced with the arrays of bismuth germanate (BGO) crystals. The distance separating the crystals is adjustable. Since the attenuation coefficient of breast tissue and the plastic compression plates is almost the same, the attenuation path can be determined from the angle of the line of response. Once the individual crystal efficiencies are calibrated, each event can be weighted by the calibration factors for that crystal pair and the attenuation path and back-projected onto many possible planes through the breast. These can all be displayed during the study giving a real time display of the activity at different layers. The use of biplanar detectors was reported by Muehllehner *et al.*[15] in 1976. The application of a small dedicated instrument for imaging the compressed breast using positron-emitting radio-pharmaceuticals has not previously been described.

II. MATERIALS AND METHODS

This feasibility study consisted of three parts:

(A) experiments with breast phantom in a conventional PET scanner;

(B) Monte Carlo simulations of proposed scanner;

(C) spatial resolution experiments.

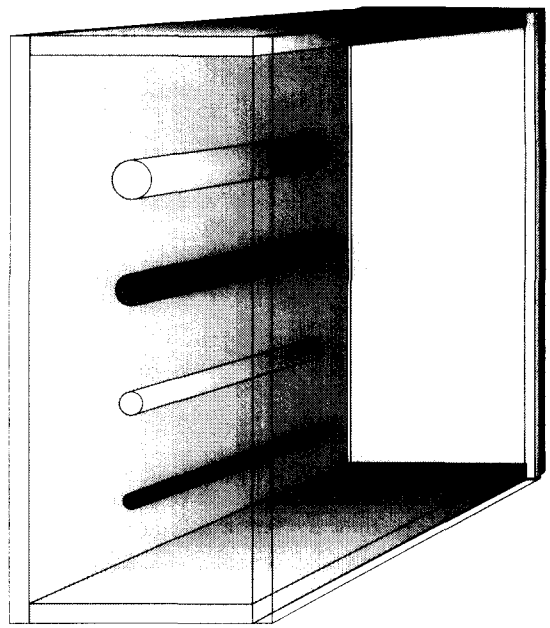

FIG. 2. Geometry and location of hot and cold rods in breast phantom. The phantom measures 137×52×140 mm inside. The rods are removable and interchangeable, with internal diameters from 2–10 mm.

A. Breast phantom

The breast phantom consists of a hollow acrylic box 137 ×52×140 mm inside dimensions and is shown in Fig. 2. It is made from 5-mm-thick clear acrylic sheet. A removable lid has tapped holes for four removable hollow glass rods of 10-, 8-, 6-, and 4-mm i.d. The outer volume of the phantom and the hollow rods can be filled independently with any desired concentration of radioactive material. The tube inserts are 100 mm long, providing a region below the tubes containing just the background solution.

Radioactive solution obtained from a ^{68}Ga (EDTA) generator was mixed and divided into two approximately equal parts by volume. One part was mixed with distilled water in the outer volume of the phantom to serve as a background corresponding to normal breast tissue activity. The other part was diluted with water to 133 ml. This solution was added to the 8- and 4-mm-diam tubes to simulate lesions with high metabolic activity. The 10- and 6-mm tubes were filled with water to provide cold spots to characterize the image quality. The activity concentrations at start of scan were 7.5 kBq/cc in the background and 70 kBq/cc in the hot cylinders.

1. Scanning procedure

The breast phantom images and profile derivations were obtained by scanning the breast phantom in the Scanditronix PC2048B brain scanner at the Montreal Neurological Institute.[16] This scanner acquires 15 slices 6.3 mm thick (FWHM) from an axial field of view of 100 mm. For these experiments the data were acquired and reconstructed for a 250-mm-diam circle. All experiments were performed in the stationary mode (non-wobbled), which can achieve an image resolution of 6 mm FWHM in the field of view of interest in these studies.

The phantom was mounted in the scanning tunnel so as to make the tubes horizontal, and extend through only slices 8–15. Slices 5 and 6 were between the ends of the tubes and the base plate, and thus contained a uniform activity distribution. A blank scan was performed just before the emission scans, and a transmission scan was performed after all the emission scans were completed. To cover the widest range of likely activity concentrations a scanning schedule was determined such that (neglecting scanner dead time and random counts) each frame would contain half the counts in the previous scan. The frame times were: 3208, 2648, 1967, 1301, 778, 430, 227, and 117 s.

2. Reconstruction of images

All slices from each data frame were reconstructed with the Scanditronix standard software. Attenuation was corrected using the transmission scan obtained at the end of the scanning sequence, and the usual corrections for scatter, randoms, and dead time were performed. A 5-mm Hanning filter was used, providing an in-plane resolution of 6 mm FWHM.

3. Extraction of limited angle projections

Selected frames were also reconstructed with a modified form of the reconstruction program which extracts the total count projections at each angle after they have been corrected for detector pair efficiency, random counts, and geometric distortions. These projections were processed by a program which allows one to select any set of projections, and sum them. These were then written to a file which can be displayed or plotted.

4. Data analysis

The range of activity concentrations and counts obtained exceeds the range of FDG concentrations and counts anticipated in actual breast scanning. Since the proposed breast imaging system will not reconstruct images but only obtain data from one or a small range of projections, we can compare the "detectability" of a hot or cold spot in the reconstructed images and the projections. There are three important differences between these studies and anticipated breast scanning. (1) The tubes in this study extend through the whole slice, whereas tumors will not be cylindrical. (2) The profiles and images represent planar sections; the proposed instrument may acquire data from arbitrary angles. (3) The "scatter fraction" will be higher in the proposed instrument. This will result in lower contrast in the projections.

B. Monte Carlo simulations

Monte Carlo simulations were performed using the programs called PETSIM[17] developed over the last five years in the Montreal Neurological Institute's Research Computing Laboratory. This set of programs simulates the source distribution, collimator, and detector as separate phases which are connected by compact gamma ray history files. The detected rays are tagged as to the number of times they have scattered before reaching the detector and the number of interactions within the crystal. This enables efficiency and resolution measurements to be performed.

1. Breast phantom simulation geometry

We assumed that the breast would be compressed to approximately 5-cm thickness between two plastic sheets which are 0.5 cm thick. The detectors cover only a fraction of the compressed breast. We approximated the breast with a box of low activity containing regions of higher activity. The breast phantom was a box 5 cm thick and 11×11 cm on the sides. The detectors were placed above and below the center of the breast phantom. The box was filled with ^{18}F-FDG with a concentration of 1 unit. Hot cylinders 6, 8, and 10 mm in diameter were positioned within the detector region and filled with fluid whose concentration was 5 units. The simulation of the breast phantom was run until a predetermined file size was obtained, corresponding to 1 250 000 annihilations. (The volume of the source is 605 ml, so this corresponds to less than 1 s of real time at a concentration of 8 kBq/ml, which is what one might expect 40 min after injection of 200 MBq of FDG.) This simulated phantom was then run through the collimator and detector phases of the simulation for each geometry tested. This simulation was used for efficiency and count rate measurements.

2. Production of profiles

A separate simulation of the breast phantom was performed in which the gamma ray creation angle was restricted to a random angle within ±10° of normal incidence on the planar detectors. This allowed direct comparison of the projection data obtained from simulations of the Scanditronix scanner and the planar detector array. The profile measurements were chosen by viewing only rays which are created at near-normal incidence to the crystals.

3. Simulations of breast phantom in Scanditronix scanner

The files of gamma ray histories were run through the simulated collimator and detectors of the Scanditronix PC2048-B brain scanner. The results of the sensitivity to true and scattered events assuming a 25% energy resolution and a lower energy discriminator of 350 KeV will be presented here.

4. Breast phantom in dedicated instrument with two planar detector arrays

The same gamma ray history files were run through several possible configurations of dual planar detector arrays. The results of the sensitivity to true and scattered events assuming a 15% energy resolution and a lower energy discriminator of 450 KeV will be presented here. The energy resolution and thresholds are different from those of the scanner simulation since the array of crystals on a position sensitive PMT will give much better light collection. The crystal arrays on the position sensitive PMTs were 70×70 mm, with 35×35 close packed 2×2-mm crystals. The crystal depth varied from 5–20 mm thick.

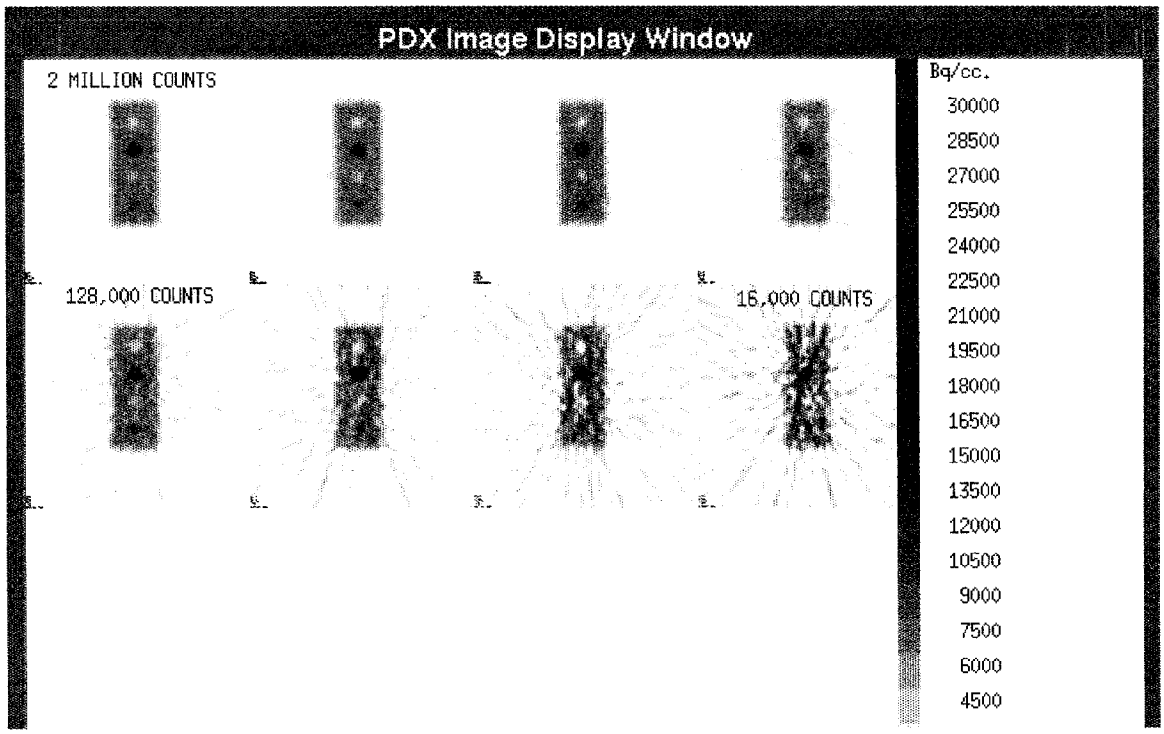

FIG. 3. Breast phantom image obtained from the Scanditronix PC2048B. The number of counts vary by a factor of 2 from one image to the next.

5. Calculation of noise-effective count rates

The effects of scattered rays, random counts, and dead time are often combined into the noise-effective count-rate (NEC) which is defined as

$$C_{\text{eff}}=\frac{T}{1+\frac{S}{T}+\frac{R}{T}},$$

where T, S, and R are the true, scattered, and random count rates including the effects of dead time, respectively. The NEC was estimated for this phantom geometry in the Scanditronix scanner and for planar crystal arrays whose crystal depth was varied from 5–20 mm.

C. Spatial resolution for very thin BGO crystals

We examined the spatial resolution of a potential system by measuring the coincidence aperture function of arrays of narrow BGO crystals. The detailed results of this work are presented elsewhere.[18,19] We measured the coincidence response of 25×10-mm BGO crystals with widths of 1–3 mm to a 0.5-mm-wide 3 μCi source of 511-keV annihilation photons. Four sets of experiments were performed with both crystals. Measurements were done with the crystals orientated with the long (25-mm axis) and short (10-mm axis) directed towards the source. Measurements were done with isolated crystals, and with the active crystals surrounded by thick BGO crystals which were not coupled to the PMT. This simulates the crosstalk from adjacent crystals which would occur in a practical array.

III. RESULTS

A. Breast phantom images

Samples taken from the background and hot regions showed activity ratio of 1:9.3. The low activity region was thus 6.1 kBq/cc and the high-activity region was 57.3 kBq/cc. This can be compared with a typical FDG brain scan where the activity in the grey matter is about 10–20 kBq/cc 40 minutes after injection of 200 MBq (about 5 mCi) of FDG. The highest reading (peak pixel in the PET image) in the 8-mm-diam tube was 28.2 kBq/cc. This is about half the actual concentration and is consistent with the image resolution of 6 mm.

Figure 3 shows images of a slice through the hot spots as the isotope decayed. The counts in each image range from 2 million in the top-left corner to 16 000 counts in the bottom right. The images shown here have been half-life corrected to the time the first scan was started to correspond to the calibrated scale on the side of the image. The early images contain more counts than one could expect from a real patient breast scan in a conventional PET scanner, since both the activity concentration and counting time are higher. Both the hot and cold spots are easily visible in image number 4 with 256 000 counts. The small (4 mm) hot spot is not visible in the 16 000 count study, which we estimate would correspond to the situation encountered with the physiological levels of breast activity[14] and a counting time of 1 min.

The images in Fig. 3 were obtained in a brain PET scanner. Multislice PET scanners used for body imaging have ring diameters about twice that of this instrument and approximately half the slice efficiency. If the same phantom

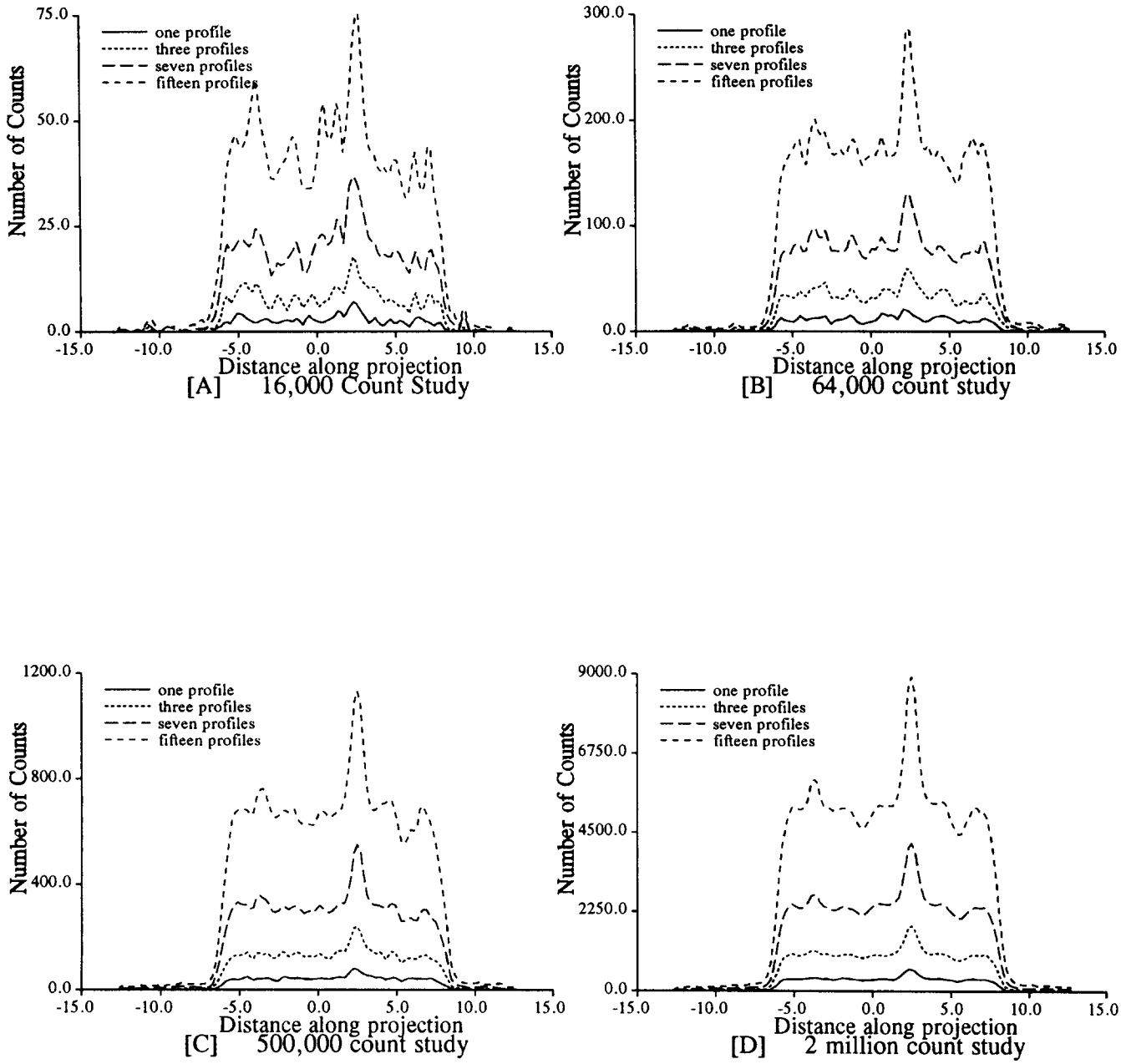

FIG. 4. Projection data in the hot and cold spot regions with total counts ranging from 16 000 (top left) to 2 million (bottom right) (from breast phantom experiment on Scanditronix PC2048B).

had been scanned in a body scanner, on a human chest there would be about a 20-fold reduction in counts due to the gamma ray attenuation in the chest. It would therefore take about 40 times longer to obtain the number of counts we obtained by scanning this phantom, alone, in a brain scanner.

B. Limited angle projections

The effect of summing several contiguous profiles on the location of hot and cold regions is shown in Figs. 4 and 5. For these two figures the data from a slice containing both hot and cold regions (Fig. 4) and another slice containing just background (Fig. 5) were subject to the same analysis. Projection #64 is plotted as a solid line and identified as "one profile" on each graph. We then added 3, then 7, then 15 contiguous profiles. The summed projections have a count ratio of 1:3:7:15. These are plotted as different line styles on each graph. The styles are consistent on each graph, and both slices are cross slices. The results are organized in the figures in order of increasing number of counts from 16 000 to 2 million. Summing the projections has the very desirable effect of increasing the detectability of both hot and cold spots.

In the data set corresponding to 2 million counts, the solid line shows only the hottest region, whereas all hot and cold spots are easily seen in the line for the sum of 15 profiles. The hot and cold spots are more easily seen in the top curve in the 64 000 count study than the bottom curve of the 2

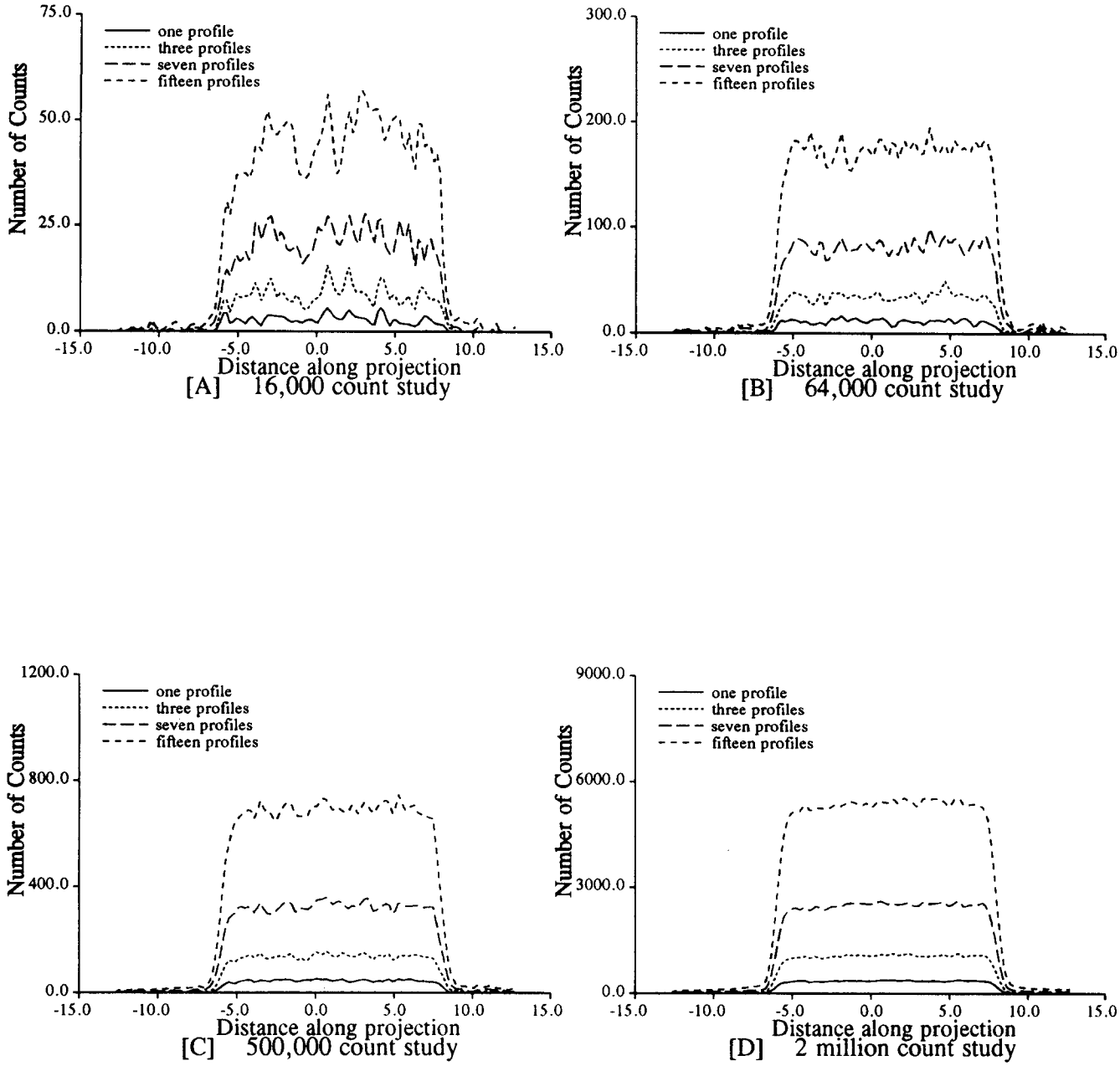

FIG. 5. Projection data in the background region with total counts ranging from 16 000 (top left) to 2 million (bottom right) (from breast phantom experiment on Scanditronix PC2048B).

million count study. The effect of summing for different angles (limited angle reconstruction) provides more useful data than counting for a much longer time from only one angle. The data in Fig. 5 provides some practical limits to the interpretation of Fig. 4 by showing how the background-only region appears for various count densities. These data appear consistent with the noise expected from Poisson statistics.

C. Monte Carlo simulations

1. Sensitivity of simulated scanner with this phantom

The profiles shown in Fig. 6(a) are for events whose gamma rays were created within 10° of vertical, in order to be consistent with the data presented below for the planar detector system. The peaks in the projection corresponds to the hot spot cylinders. These profiles represent the sum of all 15 slices.

2. Projections from very thin BGO crystals

Figure 6(b) shows the projections from planar detector arrays incorporating 5-mm-thick crystals. The three hot spots are more easily seen than in the Scanditronix data. This is due to the improved spatial resolution and the sampling of 2 mm instead of 6 mm for the brain scanner. The vertical scale of this graph can be compared with the scale of Fig. 6(a).

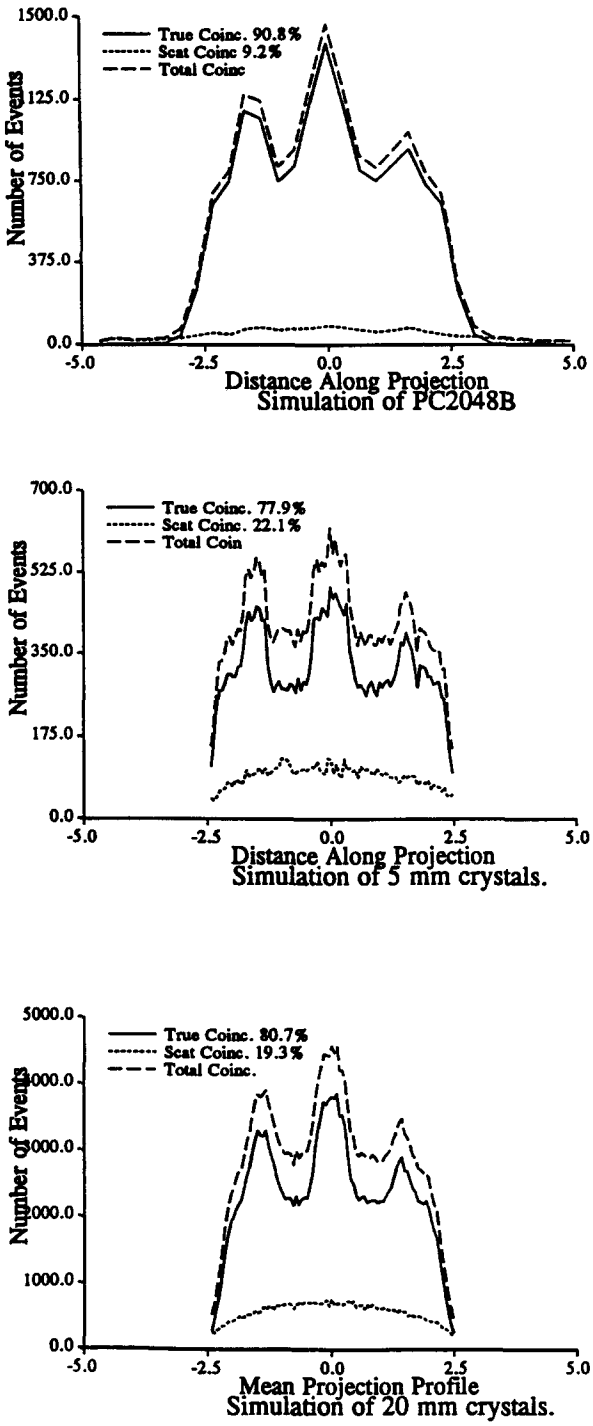

FIG. 6. Comparison of projections through simulations of breast phantom in Scanditronix scanner, and between two flat detector arrays with crystals 5 and 20 mm deep.

There are more counts per bin in this data, even though the bins are one-third as wide. This system has thus a higher efficiency per bin than the brain scanner.

3. Projections from thick BGO crystals

Figure 6(c) shows the projections from planar arrays incorporating 15-mm-thick crystals. The three hot spots are much more easily seen than in the Scanditronix data. This is due to the improved spatial resolution, and the sampling of 2 mm instead of 6 mm for the brain scanner. The vertical scale of this graph can be compared with Figs. 6(a) and 6(b). This system has thus a higher efficiency per bin than the 5-mm crystal scanner.

TABLE I. Efficiencies and scatter fractions for various systems tested.

Detector configuration	True count efficiency kcps/(μCi/cc)	Scatter percent $S/(T+S)$%	Scattered efficiency kcps/(μCi/cc)	Singles efficiency kcps/(μCi/cc)
Scanditronix	3.6	9.8%	0.36	24
5 mm thick	6.2	22.8%	1.7	97
10 mm thick	16.5	21.2%	4.3	147
15 mm thick	32.5	20.7%	8.4	213
20 mm thick	43.0	20.0%	10.7	242

4. Comparison of efficiencies for different crystal sizes

The count efficiencies (at very low count rate) are given in Table I for all configurations tested. All dual detector systems have just over twice the scatter fraction of the Scanditronix system for this imaging situation. Scatter fractions of about 20% are typical for a brain scanner used for brain imaging. The true count efficiency varies from twice that of the Scanditronix system to 12 times better as the crystal thickness is increased from 5 to 20 mm.

5. Comparison of effective count rates for different crystal sizes

The raw efficiency data of Table I must be interpreted in conjunction with the effects of noise at the higher count rates these higher efficiencies produce. The high single rates increase the dead time and the random counts. Data from all systems was plotted in Fig. 7. These NEC curves are plotted up to 18 kBq/cc in the breast phantom studied.

Based on published values of breast activities,[14] we expect activity concentrations in the range of 700–2500 Bq/cc after injection of 20 MBq. If this proves correct, effective

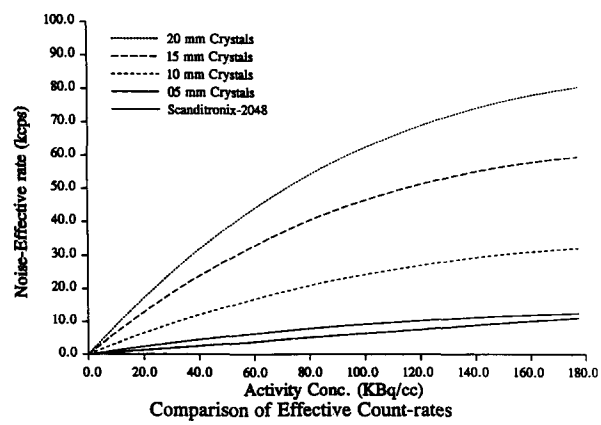

FIG. 7. Noise-effective count rate curves for breast phantom in conventional brain scanner and between two crystal matrices with depths ranging from 5–20 mm.

TABLE II. Summary of factors affecting system dead time and random rate.

System configuration	Activity for 50% dead (kBq/cc)	Trues rate: kcps for 50% dead	Singles:Coin. ratio
Scanditronix	N/A	N/A	9.3
5-mm-deep crystals	225	18.7	15.7
10-mm-deep crystals	207	43.7	8.9
15-mm-deep crystals	190	78.0	6.6
20-mm-deep crystals	190	104.2	6.5

count rates in the range of 10–30 kcps would be expected. Thus images containing a million effective counts could be obtained with the planar arrays in less than 2 min. At 20 kcps (coincident) the single count in one detector array is 66 kcps, the paralysing dead time is 16%, and the random count rate is 4 kcps. Table II is a summary of the factors affecting the system dead time and random rates.

D. Resolution experiments

The spatial resolution of pairs of identical crystals in four configurations was measured and expressed in terms of the full-width at half-maximum (FWHM) of the coincidence aperture function. Table III is a comparison of the results for 1- and 3-mm-wide crystals, separated by 12 cm. The thinner crystals provide a more than twofold improvement in the spatial resolution when the crystals are close enough to minimize the effects of noncollinearity.

IV. DISCUSSION

A. Comparison of simulations and scans

The scans on the phantom give a good impression of what the images produced by the biplanar detectors would look like if realistic size abnormalities presented an 8:1 hot spot to background ratio. The hot and cold spots are well seen in the first four images. From the expected activity concentrations (see above) it should be possible to obtain images comparable in quality to either of the last two in the top row in a 2–10-min scan. Because of the long half-life and the short imaging time, several different scan positions could be performed in a single patient sitting. In a recent article by Hunter *et al.*,[20] a breast tumor is clearly seen in a 10-min FDG scan on a Scanditronix PC4096 scanner which has half the efficiency of the PC2048.

B. Count rate limitations

Most PET systems have many small detector "blocks" made from one crystal with deep saw cuts to divide it, or from multiple crystals with partial optical coupling to the PMTs. The proposed design has only two detector arrays, rather than 128 in the Scanditronix PC-2048B with which the system is compared. To be counted, both gamma rays from each annihilation must be detected. For this to occur, both must interact with different detector blocks, and only one interaction is allowed in each, at once.

The comparison of various systems assumes the parameters in Table IV. Since the detectors are very close to the source of radiation, the resolving time can be shorter on the proposed system, since it must allow only for timing jitter in the electronics, and need not allow for the time of flight of the gamma rays. The proposed system will be much more limited by both randoms and dead time. The singles efficiency is much higher in the proposed system, and the singles:coincidence ratio is also higher.

It is important to realize that improving efficiency to true coincidence events also improves the efficiency for singles, and this increases the noise at high count rates. There are important differences between the data from a whole body scanner and the proposed detector. These and their effects on image quality are summarized in Table V. The measurements and simulations used cylindrical rods, but spheres approximate typical tumor shapes more closely. The volume of a sphere which just fits into a cylinder is 3/4 of the cylinder's volume. The observed contrast would therefore be a factor of $\frac{3}{4}$ less if the lesions were spherical.

TABLE III. Comparison of the spatial resolution of 3- and 1-mm-wide crystals.

Detector size (mm)	FWHM of coincidence aperture function (mm)			
	Long single[a]	Short single[b]	Long three[c]	Short three[d]
25×10×3	2.31	2.24	3.19	2.93
25×10×1	0.97	0.94	1.35	1.23

[a]Long single: Isolated crystals, rays incident along 25 mm axis.
[b]Short single: Isolated crystals in coincidence, rays incident along 10 mm axis.
[c]Long three: One crystal coupled and between two passive crystals, rays incident along 25 mm axis.
[d]Short three: One crystal coupled and between two passive crystals, rays incident along 10 mm axis.

C. Spatial resolution comparison

Improvement in spatial resolution can be realized using thinner crystals than those previously used in PET. This suggests that for the geometry chosen, where the crystals are close enough to minimize the effects of gamma ray noncollinearity, the spatial resolution will be dominated by the crystal size chosen. These experiments were done with the rays directed along the crystal axis, and in the actual instrument the rays will penetrate at quite steep angles. This will blur the images due to uncertainty caused by the ray's path traversing more than one crystal.

This blurring effect can be minimized at the expense of efficiency by using shorter crystals. The data in Fig. 6 comparing the simulations of the present scanner and the pro-

TABLE IV. Critical factors which control efficiency and noise at high count rates.

Scanner type	Number of detector blocks	Coincidence resolving time (ns)	Paralyzing dead time (μs)	Crystal sep. (cm)
Scanditronix PC2048	128	6	2	53
Typical body scanner	512–768	8	1	80–100
Proposed system	2	5	1	10

TABLE V. Comparison of whole body PET and proposed flat detector arrays.

Effect	Whole body (PET)	Planar array	Result/Significance
Scatter	Low	High	Reduced contrast
Efficiency	Low	Very high	Shorter image time
3-D acquisition	Currently mostly in brain imaging	Yes	More counts More angles
Crystal size	Big: (3×6×30 to 6×12×30 mm)	Small: (2×2×10 to 3×3×20 mm)	Fewer counts/detector Isotropic sampling Better image resolution
Efficiency scaling	Scales with (# of crystals)	Scales with (# of crystals)^2	More lines of response
Attenuation of gamma rays	Very high: Use transmission scan for correction	Low: simple geometric compensation	Faster scan time Real time display

posed device show the trade-off between resolution and sensitivity. The resolution is clearly better in the array made from 5-mm-deep crystals than in the 20-mm-deep array, but the sensitivity scales on these figures differ by a factor of 7.

D. Possible detector configurations

The detector simulated here was an array of very narrow crystals whose depth was varied from 5–20 mm. The sampling size in the simulations was 2 mm. The resolution experiments were done for 1.0- and 3.0-mm crystal widths. The crystals used in this work were made to order and polished on all sides. Even with the economies of scale available with making very large numbers of crystals, the cost of manufacturing the small crystals would dominate the manufacturing cost. There are other possibilities for making the crystal arrays, such as cutting slots in a large block as is done in most commercial scanners presently. The saw cuts are about 0.3 mm wide so a greater fraction of the block is lost as more smaller crystals are cut. Further investigation is required to make a realistic detector for this device.

V. CONCLUSION

The experiments using the breast phantom in the Scanditronix PET brain scanner show that images containing easily visible hot and cold spots can be obtained using conventional reconstructions in the higher range of count densities tested. However, these images were limited by count statistics for realistic scan durations at estimated physiological levels of activity. These have been compared with single and limited-angle projections. The biggest hot spot was easily visible on single projection studies containing a wide range of count rates. In order to see the smaller hot spot and any of the cold spots, it seems necessary to view the data from several angles. Data from 15 angles each 5.3° apart appeared to provide significant contrast enhancement. Data from 15 angles demonstrated the hot spots as well as conventional image reconstruction, and the cold spots were detectable in the higher count studies.

By comparing scans and simulations of a realistic breast phantom we have estimated the imaging performance in terms of spatial resolution and counting times required to obtain clinically useful images. Due to the small bore and thick shielding, it is not possible to image a human breast alone in the type of PET scanner used here. The effects of the attenuation through the chest and greater detector separation of a body scanner would reduce the quality of conventional PET images substantially even if the volume acquisition mode (available in newer scanners) was used. The biplanar detector geometry provides a substantial efficiency improvement over a conventional brain scanner and a very substantial improvement over a whole body scanner.

The spatial resolution obtained with very thin crystals would only be realized if they are made relatively short (to prevent blurring due to parallax errors and multiple gamma ray interactions). Shorter crystals reduce the efficiency. Further work is required to investigate the cost and resolution trade-offs in different crystal configurations.

ACKNOWLEDGMENTS

We would like to thank Richard Fukasawa who helped with the imaging of the breast phantom, and Yilong Ma who modified the scanner's reconstruction program to extract the projections. Claudio Ray helped with some of the illustrations. The PETSIM program was developed under an operating grant (No. OG0036672) from the Canadian National Science and Engineering Research Council. The Montreal Neurological Institute's brain imaging center is supported by a Canadian Medical Research Council special project grant (No. SP30). We acknowledge the encouragement of Dr. Henry Wagner in many discussions concerning the clinical relevance of the project. A device development is underway which is covered under US patent 5252830 and another application is pending.

[1]E. L. Nickoloff, E. Donelly, L. Eve, J. V. Atherton, and T. Asch, "Influence of focal spot intensity distribution and geometry," Med. Phys. **17**(3), 445 (1990).

[2]*Christensen's Physics of Diagnostic Radiology*, edited by T. S. Curry III, J. E. Dowdy, and R. C. Murry (Lea & Febiger, Malvern, PA, 1990), pp. 287.

[3]R. L. Wahl, R. L. Cody, G. D. Hutchins, and E. E. Mudgett, "Primary and metastatic breast carcinoma: initial clinical evaluation with PET with the radiolabeled glucose analogue 2-[F-18]-Fluoro-2-deoxy-D-glucose," Radiology **179**(3), 765–770 (1991).

[4]H. Minn and I. Soini, "[18-F] Fluorodeoxyglucose scintigraphy in diagnosis and follow up of treatment in advanced breast cancer," Eur. J. Nucl. Med. **15**, 61–66 (1989).

[5]K. Kubota, T. Matsuzawa, T. Amemiya, M. Kondo, T. Fujiwara, S. Watanuki, M. Ito, and T. Ido, "Imaging of breast cancer with [^{18}]Fluorodeoxyglucose and positron emission tomography," J. Comput. Assist. Tomogr. **13**, 6 (1989).

[6]M. A. Mintun, M. J. Welch, B. A. Seigel, C. J. Mathais, J. W. Brodack, A. H. McGuire, and J. A. Katzenellenbogen, "Breast cancer:PET imaging of oestrogen receptors," Radiology **169**(1), 45–48 (1988).

[7]Siemens/IBA CYCLONE 18/9.

[8]Scanditronix/GEMS PET-trace.

[9]F. Dehdashti, A. H. McGuire, H. F. Van Broclin, B. A. Seigel, D. P. Andriole, L. K. Griffeth, M. G. Pomper, J. A. Katzenellenbogen, and M. J. Welch, "Assessment of 21-[^{18}F]Fluoro-16(alpha)-Ethyl-19-Norprogesterone as a positron-emitting radiopharmaceutical for the detection of progestin receptors in human breast carcinomas," J. Nucl. Med. **32**, 1532–1537 (1991).

[10]A. H. McGuire, F. Dehdashti, B. A. Seigel, A. P. Lyss, J. W. Brodack, C. J. Mathais, M. A. Mintun, J. A. Katzenellenbogen, and M. J. Welch, "Positron tomographic assessment of 16 (alpha)-[^{18}F]Fluoro-17 (beta)-Estradiol uptake in metastatic breast carcinoma," J. Nucl. Med. **32**, 1526–1531 (1991).

[11]A. Verhagen, P. H. Elsinga, T. J. de Groot, A. M. Paans, C. J. de Goeij, M. Sluyser, and W. Vaalburg, "A fluorine-18 labeled progestin as an imaging agent for progestin receptor positive tumours with positron emission tomography," Cancer Res. **51**, 1930–1933 (1991).

[12]J. J. Frost, "Receptor localization and quantification with PET," Radiology **169**, 273–274 (1988).

[13]D. Carter, "Margins of lumpectomy for breast cancer," Human Pathol. **17**(4), 330–332 (1986).

[14]E. E. Kim, B. T. Kim, T. P. Haynie, D. A. Podoloff, W. H. Wong, D. J. Yang, R. S. Tilbury, G. Hortobagyi, and S. Singletary, "Evaluation of preoperative chemotherapy with loco-regionally advanced breast cancer using 18-F FDG," J. Nucl. Med. **33**(5), 828 (1992).

[15]G. Muehllehner, M. P. Buchin, and J. H. Dudek, "Performance parameters of a positron imaging camera," IEEE Trans. Nucl. Sci. **NS-23**, 528–537 (1976).

[16]A. C. Evans, C. J. Thompson, S. Marrett, E. Meyer, M. Mazza, S. Holte, R. Weltman, and T. Ericson, "Performance evaluation of the PC2048,a new 15-slice encoded-crystal PET scanner for neurological studies," IEEE Trans Med. Imag. **10**(1), 90–98 (1991).

[17]C. J. Thompson, J. Moreno-Cantu, and Y. Picard, "PETSIM: Monte Carlo simulation of all sensitivity and resolution parameters of positron imaging systems," Phys. Med. Biol. **37**(3), 731–749 (1992).

[18]K. Murthy, "A study of the effects of detector width and depth on spatial resolution in PET," M. Sc. Thesis McGill University (1993).

[19]K. Murthy, C. J. Thompson, I. N. Weinberg, and F. M. Mako, "Measurement of the coincidence response of very thin BGO crystals," submitted to IEEE Transactions on NS (1993).

[20]G. J. Hunter, N. C. Chio, T. C. McLoud, and A. J. Fischman, "Lung tumour metastasis to breast detected by F-18-fluorodeoxyglucose PET," J. Nucl. Med. **34**(9), 1571–1573 (1993).